Diagnosing the influence of diabatic processes on the explosive deepening of extratropical cyclones

Andreas H. Fink,[1] Susan Pohle,[1] Joaquim G. Pinto,[1] and Peter Knippertz[2]

Received 20 January 2012; revised 7 March 2012; accepted 7 March 2012; published 12 April 2012.

[1] A novel version of the classical surface pressure tendency equation (PTE) is applied to ERA-Interim reanalysis data to quantitatively assess the contribution of diabatic processes to the deepening of extratropical cyclones relative to effects of temperature advection and vertical motions. The five cyclone cases selected, Lothar and Martin in December 1999, Kyrill in January 2007, Klaus in January 2009, and Xynthia in February 2010, all showed explosive deepening and brought considerable damage to parts of Europe. For Xynthia, Klaus and Lothar diabatic processes contribute more to the observed surface pressure fall than horizontal temperature advection during their respective explosive deepening phases, while Kyrill and Martin appear to be more baroclinically driven storms. The powerful new diagnostic tool presented here can easily be applied to large numbers of cyclones and will help to better understand the role of diabatic processes in future changes in extratropical storminess. **Citation:** Fink, A. H., S. Pohle, J. G. Pinto, and P. Knippertz (2012), Diagnosing the influence of diabatic processes on the explosive deepening of extratropical cyclones, *Geophys. Res. Lett.*, *39*, L07803, doi:10.1029/2012GL051025.

1. Introduction

[2] Intense cyclones, associated with strong winds and sometimes extreme precipitation, are typical of the mid-latitude winter climate. Recent European wind storms like "Kyrill" in January 2007 [*Fink et al.*, 2009] and "Klaus" in January 2009 [*Liberato et al.*, 2011] led to a large number of fatalities and insured losses of several billion € [*Aon-Benfield*, 2010], as well as to a significant disruption of social activities, public transportation, and energy supply. Large-scale environmental conditions conducive to their development include an unusually strong baroclinic zone associated with an intense jet stream over an extensive longitudinal sector of the North Atlantic [*Pinto et al.*, 2009]. This is particularly true for extreme cyclones, which typically originate off the east coast of North America and propagate towards northern Europe, while secondary developments over the south-eastern North Atlantic are often more "low-level" forced [*Dacre and Gray*, 2009]. The latter suggests a more important contribution from latent heating to rapid cyclogenesis in line with ideas of so called diabatic Rossby waves or vortices [*Parker and Thorpe*, 1995; *Wernli et al.*, 2002; *Moore and Montgomery*, 2005]. In fact, latent heat release and moisture advection from the subtropics apparently played a significant role in the development of storm Klaus in January 2009 [*Knippertz and Wernli*, 2010; *Liberato et al.*, 2011]. *Ulbrich et al.* [2001] and *Pinto et al.* [2009] have shown that strong extratropical cyclones over the Atlantic Ocean are often flanked at their equatorward side with extreme values of the equivalent potential temperature, θ_e, at 850 hPa. This has commonly been interpreted as an indicator of important contributions from latent heat release to cyclone intensification.

[3] The quantification of the relative roles of dry baroclinic vs. moist diabatic processes on the development of the most destructive cyclones is a long standing issue [*Chang et al.*, 1984; *Sanders*, 1986; *Wernli et al.*, 2002]. While sensitivity studies using numerical weather prediction (NWP) models can give helpful indications for single cases, a diagnostic framework is needed that can be applied to a wide range of observational and modeling data in various spatial and temporal resolutions. We propose here a novel approach that is based on a careful evaluation of a modified version of the classical pressure tendency equation (PTE) and apply it to five recent strong and destructive European winter storms.

2. Data and Cyclone Tracking

[4] This study is based on ERA Interim Reanalysis data from the European Centre for Medium-Range Weather Forecasts [*Dee et al.*, 2011]. Atmospheric fields were extracted in full temporal (6-hourly) and spatial resolutions (T255; corresponding to a 0.75° grid spacing). Data from the 60 model levels were interpolated onto pressure levels with a vertical spacing of 10 hPa. A standard cyclone detection and tracking scheme based upon the Laplacian of mean sea-level pressure [*Pinto et al.*, 2005] was employed to determine the 6-hourly positions of the surface cyclones.

[5] The diagnostic approach is largely based on the PTE as formulated by *Knippertz and Fink* [2008], and *Knippertz et al.* [2009], which considers a vertical column from the surface to an upper boundary at pressure p_2, here chosen to be 100 hPa (see auxiliary material for more details):[1]

$$\underbrace{\frac{\partial p_{sfc}}{\partial t}}_{Dp} = \underbrace{\rho_{sfc}\frac{\partial \phi_{p_2}}{\partial t}}_{D\phi} + \underbrace{\rho_{sfc}R_d\int_{sfc}^{p_2}\frac{\partial T_v}{\partial t}d\ln p}_{ITT} + \underbrace{g(E-P)}_{EP} + RES_{PTE} \quad (1)$$

where p_{sfc} is surface pressure, ρ_{sfc} is surface air density, ϕ_{p_2} geopotential at p_2, R_d the gas constant for dry air, T_v the virtual temperature, and g the gravitational acceleration. From left to right the terms denote the surface pressure tendency

[1]Institute for Geophysics and Meteorology, University of Cologne, Cologne, Germany.
[2]School of Earth and Environment, University of Leeds, Leeds, UK.

0094-8276/12/2012GL051025

[1]Auxiliary materials are available in the HTML. doi:10.1029/2012GL051025.

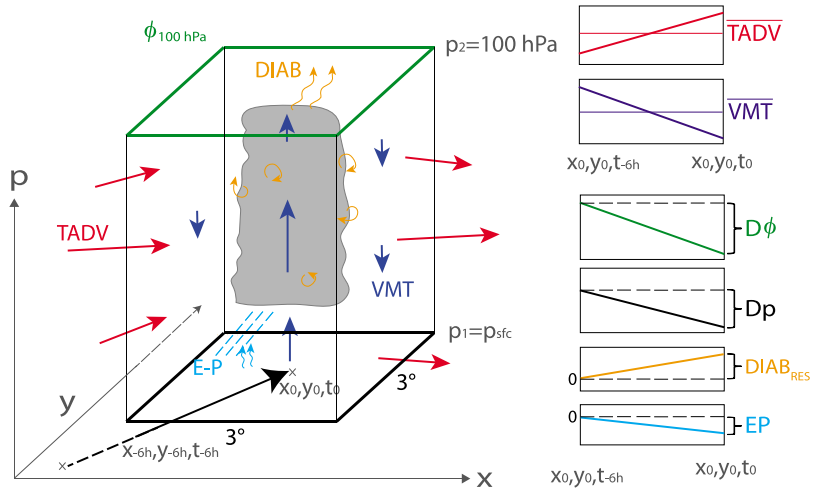

Figure 1. Schematic illustration of the methodology (see Section 2 for details and definition of terms). The bold arrow in the x-y plane indicates the motion of the center of a surface cyclone between two analysis times t_0 and t_{-6h} (arrow length not true to the scale). The surface pressure tendency equation is evaluated for the 3° × 3° latitude-longitude box extending from the surface to 100 hPa centered on the position of the storm at t_0. The terms of equation (2), TADV (horizontal advection; red arrows) and VMT (vertical advection; dark blue vectors), are computed by integrating over the box volume and then averaging over t_0 and t_{-6h} as schematically indicated in the two graphs in the top right corner. The computation of the terms $D\phi$, Dp, DIAB (diabatic processes; curled orange vectors), and EP (evaporation minus precipitation; curled blue vectors and dashed blue lines) is illustrated in the lower four graphs on the right-hand side. Note that while $D\phi$ and Dp are simple differences between instantaneous values at t_0 and t_{-6h}, EP is the difference between two parameters accumulated between t_0 and t_{-6h}. $DIAB_{RES}$ is the residuum of equation (2).

(Dp), the change in geopotential at the upper boundary ($D\phi$), the vertically integrated virtual temperature tendency (ITT), the mass loss (increase) by surface precipitation P (evaporation E; EP), and a residuum due to discretization (RES_{PTE}). With all other terms zero, a lowering of the upper boundary ($D\phi$) causes surface pressure fall, as it must be associated with mass evacuation by divergent winds. If the column height remains constant, warming results in horizontal expansion and therefore in a loss of mass (i.e., surface pressure fall). In reality a combination of the two processes is typically found (Figure S1 in the auxiliary material).

[6] The ITT term in equation (1) can then be further expanded to (see auxiliary material):

$$\begin{aligned} ITT = &+ \rho_{sfc} R_d \int_{sfc}^{p_2} -\vec{v}\cdot\vec{\nabla}_p T_v d\ln p && (TADV)\\ &+ \rho_{sfc} R_d \int_{sfc}^{p_2} \left(\frac{R_d T_v}{c_p p} - \frac{\partial T_v}{\partial p}\right)\omega\, d\ln p && (VMT)\\ &+ \rho_{sfc} R_d \int_{sfc}^{p_2} \frac{T_v Q}{c_p T} d\ln p && (DIAB)\\ &+ RES_{ITT}, && (2) \end{aligned}$$

where T is temperature, $\vec{v}$ and ω the horizontal and vertical wind components, c_p the specific heat capacity at constant pressure, and $\dot{Q}$ the diabatic heating rate. The first and second terms on the right hand side describe the effects of horizontal temperature advection (TADV) and vertical motions (VMT) on the column-integrated temperature tendency. DIAB contains the influence of diabatic processes such as radiative warming/cooling, latent heat release due to phase changes of water, diffusion, and dissipation. In cloudy areas, like in the core region of extratropical storms, the latent heat release related to microphysical cloud and convective processes is the most important contribution to DIAB, resulting in an atmospheric warming and pressure fall. The term RES_{ITT} represents errors due to discretizations in time and space. The ITT term also includes a small term arising from changes in the humidity content in the column, which is neglected here for reasons explained in the auxiliary material.

[7] The application of equations (1) and (2) using 6-hourly ERA-Interim data is illustrated in Figure 1. The p_{sfc} change between t_{-6h} and t_0 is evaluated over a 3° × 3° latitude-longitude box centered on the position of the surface cyclone at t_0. All other terms in equations (1) and (2) with time tendencies (Dp, $D\phi$, and ITT) are also calculated for this box as area- or volume-averaged changes between t_0 and t_{-6h}. The two instantaneous terms (TADV, VMT) are computed by integration over the box volume and then averaging over t_{-6h} and t_0 (Figure 1). This averaging procedure yielded the smallest residua in equation (2) for an application to the West African heat low using AMMA re-analysis data, for which diabatic tendencies are available [*Pohle*, 2010]. The box is moved along the storm track during the lifetime of the cyclone to create a time series.

[8] Since ERA-Interim does not provide any diabatic tendencies, DIAB had to be calculated as the residuum of equation (2) and is therefore termed $DIAB_{RES}$. While clearly a limitation of this approach, tests using explicit heating rates show that DIAB and $DIAB_{RES}$ are usually rather similar, though $DIAB_{RES}$ also contains contributions from RES_{ITT} (see auxiliary material and *Pohle* [2010]). Further tests varying the upper integration boundary p_2 and the size of the box show that the method is robust (see auxiliary material). Finally, the relative contribution of $DIAB_{RES}$ to the total pressure tendency, $DIAB_{ptend}$, is defined by

$$DIAB_{ptend} = \begin{cases} \dfrac{|DIAB_{RES}|}{|TADV| + |VMT| + |DIAB_{RES}|} * 100,\ sgn\ (DIAB_{RES}) = \text{sgn (TADV)} = \text{sgn (VMT)} \\ \dfrac{|DIAB_{RES}|}{|TADV| + |DIAB_{RES}|} * 100,\ sgn\ (DIAB_{RES}) = \text{sgn (TADV)}\ \wedge\ sgn\ (DIAB_{RES}) \neq \text{sgn (VMT)}. \\ \dfrac{|DIAB_{RES}|}{|VMT| + |DIAB_{RES}|} * 100,\ sgn\ (DIAB_{RES}) = \text{sgn (VMT)}\ \wedge\ sgn\ (DIAB_{RES}) \neq \text{sgn (TADV)} \end{cases} \quad (3)$$

3. Selection of Storms

[9] The five European winter storms selected to test our methodology are Lothar, Martin (both in December 1999), Kyrill I and II (January 2007, note that Kyrill underwent secondary cyclogenesis over the Atlantic Ocean and thus consists of two cyclone life cycles [*Fink et al.*, 2009]), Klaus (January 2009), and Xynthia (February 2010). All underwent explosive cyclogenesis over the North Atlantic Ocean (see auxiliary material) and brought considerable damage to western and central Europe [*Ulbrich et al.*, 2001; *Fink et al.*, 2009; *Liberato et al.*, 2011]. The west-east evolutions of the core mean-sea level pressure as the storms cross the Atlantic Ocean are shown in Figure 2 together with track maps of 300-hPa wind speed and 850-hpa θ_e in a longitudinal moving window centered on the 6-hourly surface position of the storms. All storms (Figures 2a, 2d, 2g, and 2j) except Xynthia (Figure 2m) are associated with a strong polar jet with wind speeds in excess of 160–180 kn, indicating strong baroclinicity. The former storms underwent explosive cyclogenesis during the crossing of the jet polewards (Table S1 and Figures S4–S7 in the auxiliary material). Lothar and Klaus are known examples of storms that came under an area of jet-induced upper-level divergence after entering the left exit region while undergoing explosive deepening [*Ulbrich et al.*, 2001; *Liberato et al.*, 2011]. This process is well known to foster rapid development of extratropical cyclones [*Uccellini*, 1990]. Xynthia was different in that the storm never crossed the associated polar jet stream (Figure 2m); a split jet configuration might have contributed to the intensification later in its explosive development on 27 February 2010 (Figure S8 in the auxiliary material).

[10] Another factor related to intense cyclogenesis is the ingestion of low-level warm and humid air, transported towards the cyclone's centre ahead of the cold front in the warm conveyer belt [*Browning and Roberts*, 1994]. θ_e at 850 hPa is often used to indicate and track these warm and humid air masses [*Ulbrich et al.*, 2001; *Pinto et al.*, 2009]. Klaus, and especially Xynthia, were associated with extensive areas of θ_e values higher than 320 K at the time when explosive cyclogenesis started (Figures 2k and 2n). Lothar, Martin, and Kyrill I were flanked by lower values and less extensive areas of high θ_e (Figures 2b, 2e, and 2h; see also Figures S4–S8 in Text S1). These analyses allow some qualitative statements as to the potential role of diabatic forcing of the storm deepening. The relative roles of the jet stream (reflecting baroclinic processes) and diabatic heating, however, remain unclear. As will be shown in the next section, such an assessment can be achieved using the PTE.

4. Application of the PTE to Five Recent Atlantic Winter Storms

[11] The PTE analysis results are displayed for the five selected winter storms at 6-hourly intervals in Figure 3. The black lines in the left panels show the time evolution of Dp along the storm tracks over the time periods given in the captions of Figure 2. The corresponding segments of the cyclone tracks are colored in the track map shown in Figure S3 in Text S1. It is interesting to compare the evolution of Dp in Figures 3a–3e to Figures 2c, 2f, 2i, 2l, and 2o as well as to Table S1 in Text S1. Despite the difference in physical meaning (the latter shows the longitudinal evolution of the core pressures of the cyclone while the former shows the change in pressure in a box fixed in space during the 6 hours the cyclone is approaching) there are some clear structural similarities. This is most obvious for Martin, which deepened only slightly on 25 and 26 December 1999 (Figure 2f) associated with small values of Dp (Figure 3b). On 27 and 28 December the storm went through a period of rapid deepening and subsequent filling, which is well matched by the sharp decrease and subsequent return to small values of Dp. A similarly good correspondence is found for Klaus (Figures 2l and 3d) and Xynthia (Figures 2o and 3e). For Lothar the match between core-pressure changes (Figure 2c) and Dp (Figure 3a) is more complicated due to the dramatic change in propagation speed. During early stages on 24 December 1999, when the storm is rapidly moving across the Atlantic, Dp is on the order of 10 hPa/6 h, although the core pressure is deepening rather slowly. During late stages on 27 December 1999, the cyclone is almost stationary with slowly increasing core pressure and Dp close to zero. For Kyrill the match between core pressure and Dp evolution is somewhat complicated by the two pressure centers, but even here some structural similarities are evident (Figures 2i and 3c).

[12] According to equation (1) Dp equals the sum of Dϕ, ITT, EP, and RES_{PTE}. For all storms ITT clearly dominates surface pressure changes during most of the lifetime (Figures 3a–3e). EP is usually rather small, but reaches almost 2 hPa/6 hrs on 24 December 1999 12–18 UTC (Figure 3a), which is equivalent to 20 mm of box-averaged accumulated rainfall (see auxiliary material). At this time, the RES_{PTE} term, which is negligible during most other times, is on the order of 1.3 hPa, pointing to problems with quantitative precipitation forecast in the ECMWF model. A

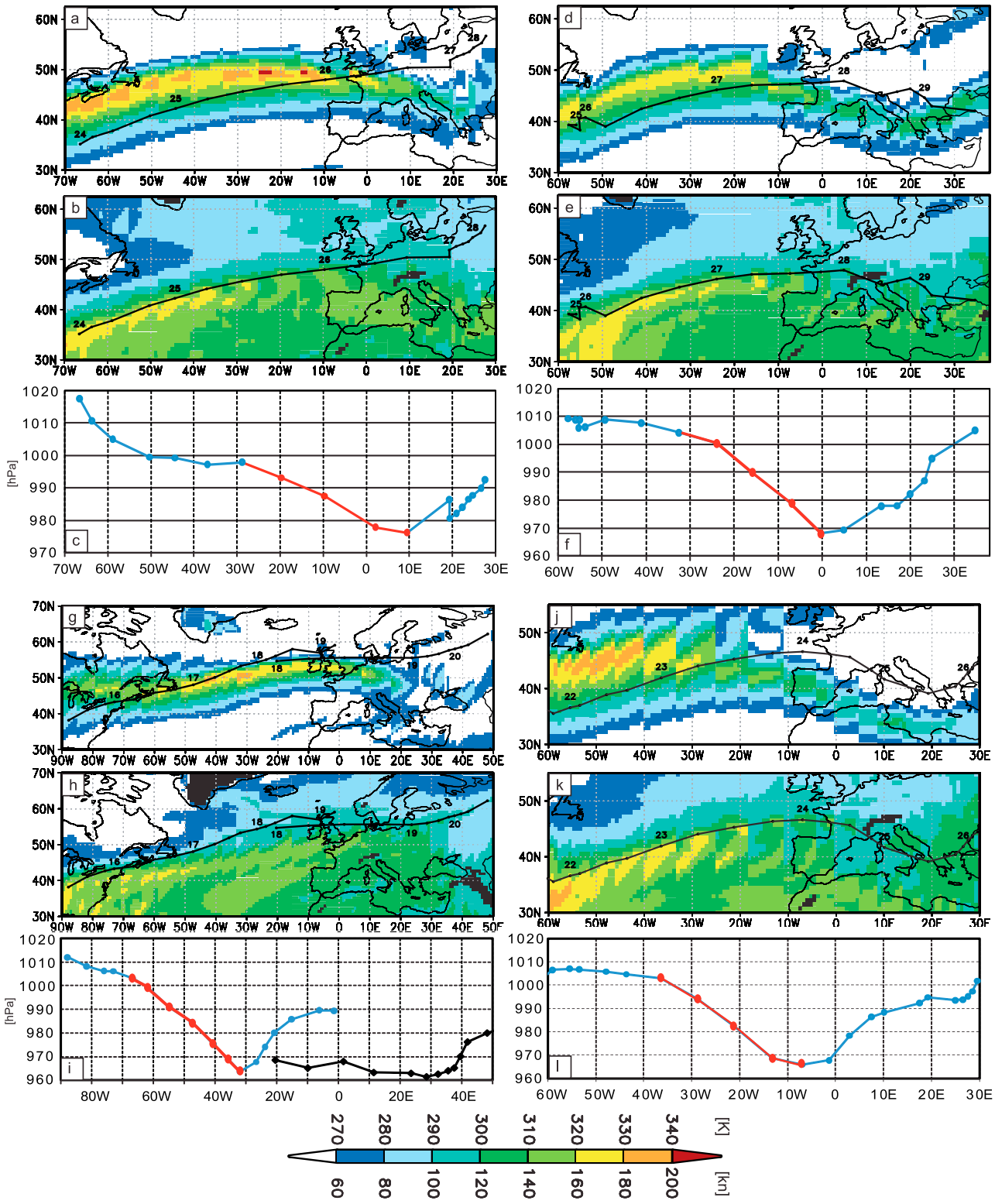

Figure 2. Characteristics of investigated storms. (a) 6-hourly track of storm Lothar between 0000 UTC 24 and 1200 UTC 28 December 1999 together with wind speed [Kn] at 300 hPa in a longitudinal window centered on the surface position of the storm. (b) As Figure 2a but for θe [K] at 850 hPa. (c) 6-hourly core pressure development of Lothar plotted against longitude. The red part of the pressure curve denotes the period of explosive deepening as in Table S1 in Text S1. Corresponding analyses for (d–f) Martin 0600 UTC 24 – 1800 UTC 29 December 1999, (g–i) Kyrill I and II 0600 UTC 15 – 1800 UTC 20 January 2007, (j–l) Klaus 1200 UTC 21 – 1800 UTC 26 January 2009, and (m–o) Xynthia 1800 UTC 25 February – 1200 UTC 03 March 2010. The calendar days along the tracks correspond to 0000-UTC positions. Note the slightly different geographical areas of the horizontal distributions.

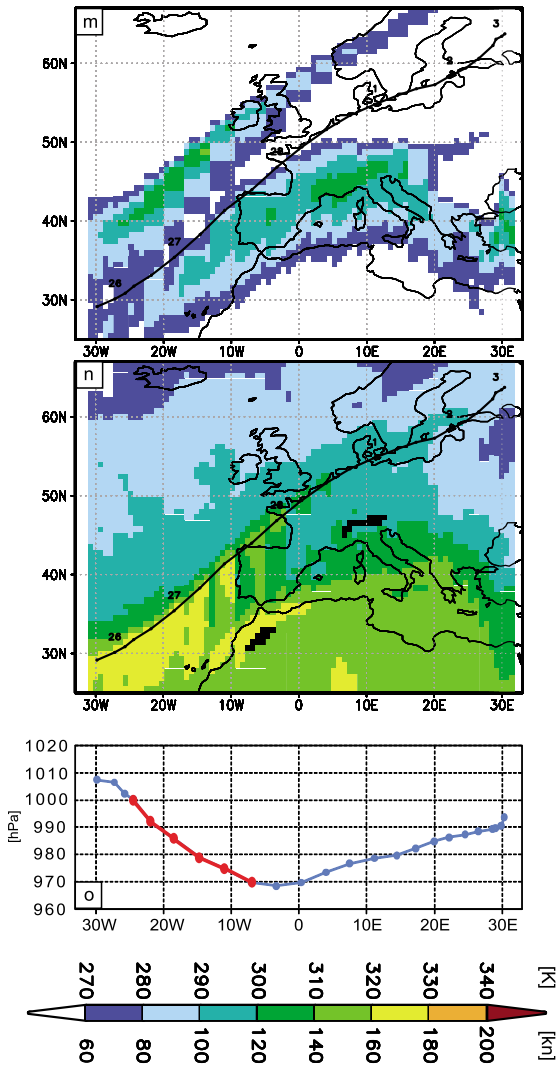

Figure 2. (continued)

similar behavior is found for the deepening phase of Xynthia (Figure 3e). Dϕ also contributes substantially during some time steps only. The most notable period is the decay of Lothar over Poland and Russia on 26 and 27 December 1999, when Dϕ is relatively large and negative over four time steps (Figure 2a). The sign of Dϕ implies a significant lowering of the 100-hPa surface, which is to some extent compensated by a cooling of the atmospheric column (positive ITT) towards the end of the period. This is in contrast to the four other storms where Dϕ is usually smaller in magnitude and positive. It is likely that this peculiar behavior of Lothar is connected with the movement into the left exit region of the extreme jet over western Europe (Figure 2a), but a detailed study is beyond the scope of this more methodological paper.

[13] Figures 3f–3j show the split of the dominant ITT term into TADV, VMT, and $DIAB_{RES}$ (see equation (2); note the different y axis compared to the left panels). Martin stands out as the system with largest and most constant contributions from VMT ranging between 20 and 40 hPa/6 h (Figure 3g), indicating ascent and adiabatic cooling. Nearly all of this is compensated by similar values of opposite sign associated with TADV. This cancellation, which is found for all other storms as well, is the consequence of air ascending on isentropic surfaces in the area downstream of the cyclone center, where warm advection dominates. Diabatic contributions ($DIAB_{RES}$) are relatively small during the early stages of Martin, but increase to more than 20 hPa/6 h during the main deepening phase on 26 and 27 December 1999, during which time they show a similar magnitude to ITT. $DIAB_{RES}$ is again closely related to VMT, as latent heating will depend on ascending motions. However, other factors such as absolute and relative humidity and vertical stability will modify the relation between the two. In order to get an estimate of the relative roles of baroclinic and diabatic contributions, the gray bars at the bottom of each panel show $DIAB_{ptend}$ as defined in equation (3). We expect $DIAB_{ptend}$ to be more robust than the absolute values of single terms, since they are dependent on factors like storm size, propagation speed, and size of the target box. Over almost all analysis times in Figure 3, $DIAB_{RES}$ is negative, thus $DIAB_{ptend}$ indicates the contribution of diabatic processes to pressure drop. For Martin, $DIAB_{ptend}$ ranges around 30% with highest values towards the end of the deepening phase. From Figure 3, it is evident that VMT is usually of opposite sign to $DIAB_{RES}$ and therefore $DIAB_{ptend}$ is generally calculated using the middle expression of equation (3). Thus about 70% of the pressure drop during Martin's explosive development is due to horizontal temperature advection, suggesting an overall baroclinically dominated development. Kyrill shows a very similar behavior, although the magnitudes of single terms are somewhat smaller, particularly for Kyrill II (Figure 3g).

[14] The other three storms, Klaus, Xynthia, and Lothar, show substantial contributions from $DIAB_{RES}$ of well above 20 hPa/6 h, leading to $DIAB_{ptend}$ terms of more than 60% due to relatively small contributions from TADV (Figures 3f, 3i, and 3j). The most impressive example is Xynthia. The large VMT values, which reach similar magnitudes as for Martin during the main deepening phase, are mainly balanced by equally large $DIAB_{RES}$ contributions, while TADV remains largely below 20 hPa/6 h (Figure 3j). This behavior is consistent with the relatively weak jet (Figure 2m) and the high θ_e values in the vicinity of the storm during 26 and 27 February 2010 (Figure 2n). Such simple reasoning, however, does not hold in detail for the other storms. Klaus for example is in the vicinity of a very intense jet on 22 January 2009 (Figure 2j), but TADV contributions are small (Figure 3i). On the other hand $DIAB_{RES}$ contributions are largest on 23 January 2009, when Klaus has already left the area of highest θ_e (Figure 2k). In addition, Lothar has the strongest jet (Figure 2a) of all cases studied here, yet TADV is relatively small throughout most of the development (Figure 3f). θ_e on the other hand is high during the early stages associated with particularly large values of $DIAB_{ptend}$, which is consistent with ideas of diabatic Rossby waves as discussed by *Wernli et al.* [2002]. These results suggests that the details of the state of development of the cyclone, the interactions with the baroclinic zone, and the actual realization of latent heating from high-θ_e air are crucially important for determining VMT, TADV, and $DIAB_{RES}$. The sole existence of a strong jet or high-θ_e

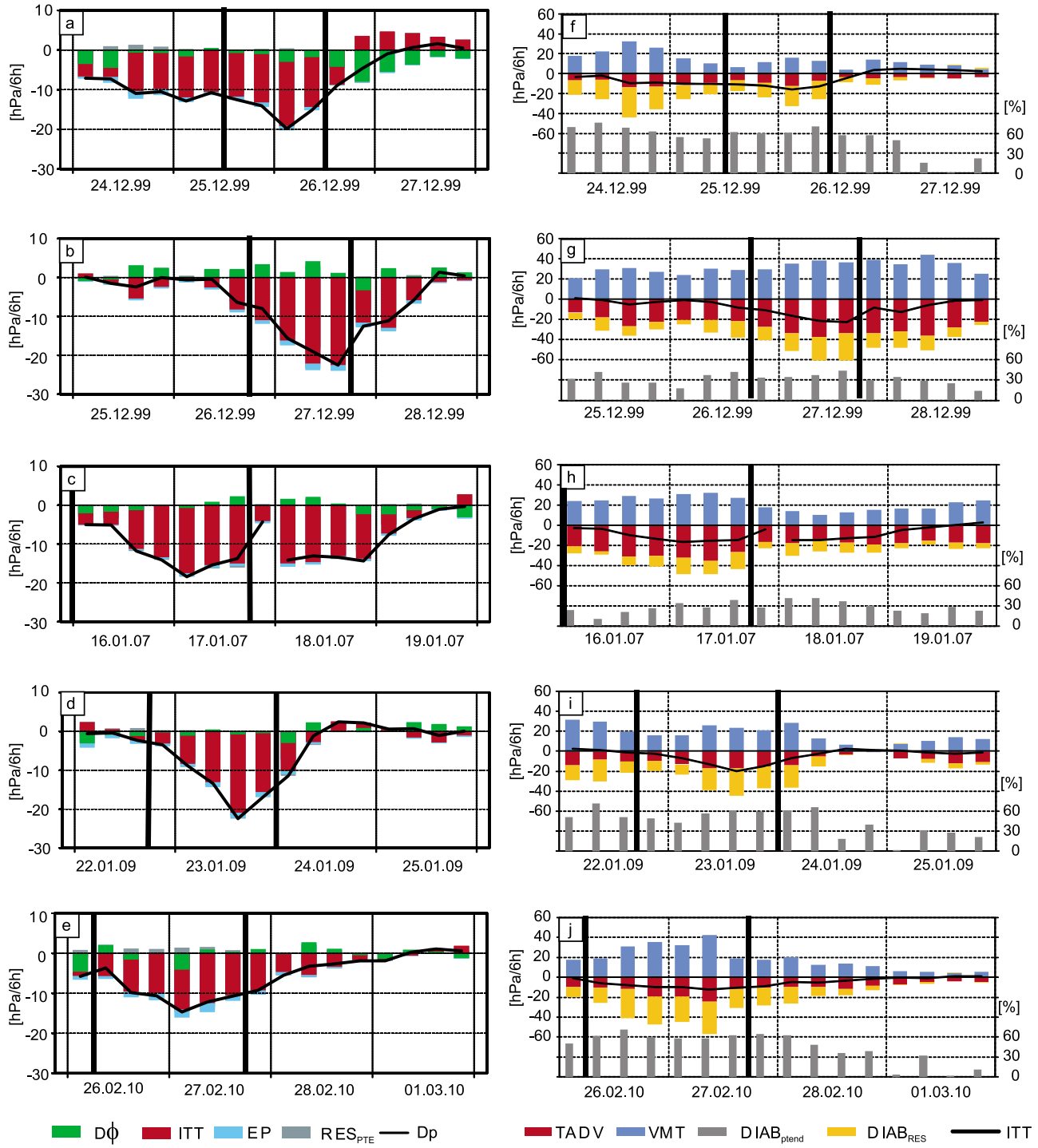

Figure 3. Results of the PTE analysis. Terms of (left) equation (1) and (right) equation (2) for the storms (a, f) Lothar, (b, g) Martin, (c, h) Kyrill I and II, (d, i) Klaus, and (e, j) Xynthia. For an explanation of the different terms, see section 2. In the right panels, $DIAB_{ptend}$ (gray bars in %, scale on right y-axis) is defined as in equation (3). Note the different pressure scales in the left and right panels. The vertical bold lines delineate the interval of explosive deepening as in Table S1 in Text S1. The periods correspond to those in the captions of Figure 2 (see also Figure S3 in Text S1).

air is not sufficient to deduce the relative roles of baroclinic vs. diabatic processes.

5. Summary and Conclusions

[15] The relative roles of baroclinic and diabatic processes for explosive deepening of extratropical cyclones have been debated for a long time, mostly on the basis of case studies. Here we presented a powerful diagnostic approach to the problem, which is based on a combination of an automatic cyclone tracking with a special version of the classical PTE that relates changes in surface pressure to contributions from horizontal temperature advection and vertical motion as well as to diabatic processes, i.e., mainly latent

heat release in clouds. Along the entire track, the PTE is evaluated in a $3^\circ \times 3^\circ$ box from the surface to 100 hPa centered on the location the storm is moving to within the next time step. The great advantage of this new approach is the easy applicability to large gridded datasets, even if diabatic tendencies are not explicitly available as in many reanalysis products.

[16] The strengths and limitations of the method are illustrated here through application to five explosively deepening winter storms over the North Atlantic Ocean (Lothar, Martin, Kyrill, Klaus, and Xynthia), which all caused considerable damage in Europe. Data used are 6-hourly ERA-Interim re-analyses. For enhanced interpretation of the results, the PTE analysis was complemented with other classical cyclogenetic factors, i.e., the strength of the polar jet and θ_e at 850 hPa in the warm sector [*Pinto et al.*, 2009]. The main conclusions from this analysis are:

[17] 1. The time evolutions of the actual core pressure of the storm and the 6-hourly pressure changes in the moving box used to evaluate the PTE show structural similarities that are dominated by the explosive deepening.

[18] 2. The pressure changes largely follow the net virtual temperature change in the box with only short periods, when vertical movements of the upper lid of the box contribute substantially, as for example during the decay of Lothar.

[19] 3. The vertical motion term (VMT) is positive throughout the entire lifecycle of all storms indicating the dominance of ascent downstream of the cyclone center.

[20] 4. VMT is (over-)compensated by negative contributions through warm temperature advection (TADV) and diabatic heating ($DIAB_{RES}$), whose relative importance vary strongly during the lifetime of the storms and from system to system.

[21] 5. Martin and Kyrill appear to be dominated by baroclinic processes with contributions of TADV to the total negative pressure tendencies of around 70%.

[22] 6. Despite comparable jet strengths, a similar track relative to the jet, and equally high θ_e values at 850 hPa in the warm sector, Lothar and Klaus show much larger diabatic contributions to the negative pressure tendency of around 60% over a 2.5 day period.

[23] 7. Xynthia stands out as a system with an unusual SW–NE track into Europe, which appears to have benefited from a complicated split jet structure in the later development stages. It is also associated with high θ_e values and shows very large diabatic contributions.

[24] 8. The PTE results indicate that θ_e in the warm sector and the jet strength alone are not sufficient to make an assessment of the relative importance of baroclinic and diabatic processes, but that a more elaborate analysis is needed to make this judgment.

[25] Future work should deepen this analysis further by looking more closely into individual times and PTE terms. Particularly for Xynthia, Klaus, and Lothar a comparison with sensitivity experiments, in which diabatic processes are suppressed in a numerical model, would be interesting to confirm the PTE results. In addition it should also be tested to what extent the diabatic term is sensitive to the model and data assimilation system by comparing with other analysis products. More studies on the sensitivity of results to storm diameter, translation speed, box size, and analysis time steps are also needed. In the long run, the PTE analysis will be applied to longer timeseries from both reanalysis and climate model data to generate robust statistics across a broader range of cyclone intensities and development types. This will for the first time allow a systematic investigation of the relative contribution of diabatic processes to storm intensification in recent and future climate conditions, going much beyond the case studies found in the literature so far.

[26] **Acknowledgments.** We thank the European Centre for Medium-Range Weather Forecasts for the use of the ERA Interim Reanalysis dataset. JGP thanks AON Benfield Impact Forecasting for support over the EUWS project. PK acknowledges funding from the AXA Research Fund for the SEAMSEW project. We wish to thank Thomas Engel, Tomek Trzeciak and Jenny Owen for help in creating Figure 3. Finally we are grateful to Steve Dorling and one anonymous reviewer for their comments that greatly helped to improve the paper.

[27] The Editor thanks Steve Dorling and an anonymous reviewer for their assistance in evaluating this paper.

References

Aon-Benfield (2010), Annual global climate and catastrophe report: Impact forecasting—2009, report, Chicago, Ill. [Available at http://www.aon.com.]

Browning, K., and N. M. Roberts (1994), Structure of a frontal cyclone, *Q. J. R. Meteorol. Soc.*, *120*, 1535–1557.

Chang, C. B., D. J. Pepkey, and C. W. Kreitzberg (1984), Latent heat induced energy transformations during cyclogenesis, *Mon. Weather Rev.*, *112*, 357–367, doi:10.1175/1520-0493(1984)112<0357:LHIETD>2.0.CO;2.

Dacre, H. F., and S. L. Gray (2009), The spatial distribution and evolution characteristics of North Atlantic cyclones, *Mon. Weather Rev.*, *137*, 99–115, doi:10.1175/2008MWR2491.1.

Dee, D., et al. (2011), The ERA-Interim reanalysis: Configuration and performance of the data assimilation system, *Q. J. R. Meteorol. Soc.*, *137*, 553–597, doi:10.1002/qj.828.

Fink, A. H., T. Brücher, E. Ermert, A. Krüger, and J. G. Pinto (2009), The European storm Kyrill in January 2007: Synoptic evolution, meteorological impacts and some considerations with respect to climate change, *Nat. Hazards Earth Syst. Sci.*, *9*, 405–423, doi:10.5194/nhess-9-405-2009.

Knippertz, P., and A. H. Fink (2008), Dry-season precipitation in tropical West Africa and its relation to forcing from the extratropics, *Mon. Weather Rev.*, *136*, 3579–3596, doi:10.1175/2008MWR2295.1.

Knippertz, P., and H. Wernli (2010), A Lagrangian climatology of tropical moisture exports to the Northern Hemispheric extratropics, *J. Clim.*, *23*, 987–1003, doi:10.1175/2009JCLI3333.1.

Knippertz, P., A. H. Fink, and S. Pohle (2009), Reply, *Mon. Weather Rev.*, *137*, 3151–3157, doi:10.1175/2009MWR3006.1.

Liberato, M. R. L., J. G. Pinto, I. F. Trigo, and R. M. Trigo (2011), Klaus—An exceptional winter storm over northern Iberia and southern France, *Weather*, *66*, 330–334, doi:10.1002/wea.755.

Moore, R. W., and M. T. Montgomery (2005), Analysis of an idealized, three-dimensional diabatic Rossby vortex: A coherent structure of the moist baroclinic atmosphere, *J. Atmos. Sci.*, *62*, 2703–2725, doi:10.1175/JAS3472.1.

Parker, D. J., and A. J. Thorpe (1995), Conditional convective heating in a baroclinic atmosphere: A model of convective frontogenesis, *J. Atmos. Sci.*, *52*, 1699–1711, doi:10.1175/1520-0469(1995)052<1699:CCHIAB>2.0.CO;2.

Pinto, J. G., T. Spangehl, U. Ulbrich, and P. Speth (2005), Sensitivities of a cyclone detection and tracking algorithm: Individual tracks and climatology, *Meteorol. Z.*, *14*, 823–838, doi:10.1127/0941-2948/2005/0068.

Pinto, J. G., S. Zacharias, A. H. Fink, G. C. Leckebusch, and U. Ulbrich (2009), Factors contributing to the development of extreme North Atlantic cyclones and their relationship with the NAO, *Clim. Dyn.*, *32*, 711–737, doi:10.1007/s00382-008-0396-4.

Pohle, S. (2010), Synoptische und dynamische Aspekte tropisch-extratropischer Wechselwirkungen: Drei Fallstudien von Hitzetiefentwicklungen über Westafrika während des AMMA-Experiments 2006 [in German], PhD thesis, Univ. of Cologne, Cologne, Germany. [Available at http://kups.ub.uni-koeln.de/volltexte/2010/3157/pdf/DissertationSusanPohle2010.pdf.]

Sanders, F. (1986), Explosive cyclogenesis in the west-central North Atlantic Ocean, 1981–84. Part I: Composite structure and mean behavior, *Mon. Weather Rev.*, *114*, 1781–1794, doi:10.1175/1520-0493(1986)114<1781:ECITWC>2.0.CO;2.

Uccellini, L. W. (1990), Process contributing to the rapid development of extratropical cyclones, in *Extratropical Cyclones: The Eric Palmen Memorial Volume*, edited by C. Newton and E. Holopainen, pp. 81–107, Am. Meteorol. Soc., Boston, Mass.

Ulbrich, U., A. H. Fink, M. Klawa, and J. G. Pinto (2001), Three extreme storms over Europe in December 1999, *Weather*, *56*, 70–80.

Wernli, H., S. Dirren, M. A. Liniger, and M. Zillig (2002), Dynamical aspects of the life-cycle of the winter storm 'Lothar' (24–26 December 1999), *Q. J. R. Meteorol. Soc.*, *128*, 405–429, doi:10.1256/003590002321042036.

A. H. Fink, J. G. Pinto, and S. Pohle, Institute for Geophysics and Meteorology, University of Cologne, Kerpener Str. 13, D-50923 Cologne, Germany. (fink@meteo.uni-koeln.de; jpinto@meteo.uni-koeln.de)

P. Knippertz, School of Earth and Environment, University of Leeds, Leeds LS2 9JT, UK. (p.knippertz@leeds.ac.uk)